

Hyperspectral Nonlinear Optical Light Generation from a Monolithic GaN Microcavity

Sween Butler, Hongxing Jiang, Jingyu Lin, and Arup Neogi*

Localized spatial excitation of a single hexagonal GaN micropillar with $(1\bar{1}01)$ facets formed by selective area growth is optimized for nonlinear optical light (NLO) generation due to second harmonic generation (SHG) and multiphoton luminescence (MPL). Multiphoton transition induced ultraviolet and yellow luminescence is observed for excitations above and below half bandgap energy. SHG and MPL observed for excitations below half the bandgap energy are superimposed to realize broadband emission in the UV–visible range. The light generation is optimized by controlling the cavity modes formed by the hexagonal facets and the tip enhanced effects from the pyramid. The MPL is optimum at the apex of the pyramid. The SHG is most efficient within the pyramid ($\approx 4\ \mu\text{m}$ above the base) due to the formation of spatially stable cavity modes within the cavity. The NLO interactions within the pyramid are optimized to realize microphotonic white light sources and coherent tunable UV–visible sources using spatially controlled excitation without any change in material parameters. At the bandgap of GaN, the resonant two-photon emission dominates the nonlinear light generation process compared to the coherent SHG light generated within the cavity.

its efficiency in micro-optical systems. This work is focused on exploring a NLO material system where the multiple round trips within the microcavity can enhance the light–matter interaction due to the high Q of the cavity without increasing the device dimensions. The SHG process converts two coherent photons with frequency ω to a coherent single photon with frequency 2ω . Conversely, multiphoton transitions resulting in photoluminescence (PL) and stimulated emission under high optical field density is a third-order nonlinear process. NLO effects are generally manifested at high electron densities induced by higher power incident pump laser fluences.^[1] Due to the relative lower threshold of quadratic nonlinear processes over cubic process, the nonlinear light generation in low-dimensional semiconductor structures has been limited mainly to SHG.^[2–4] Since microcavities can be made to be resonant to input or gener-

ated beam, they can serve as platforms for power-dependent devices such as modulators or switches while maintaining their small device dimensions. The generation of light due to concurrent effects of efficient second and third-order nonlinearities in semiconductor nano- or microstructures under certain resonant conditions can result in broadband emitters or tunable coherent sources not restricted by requirements for high threshold power and can be realized under quasi-phase-matching conditions for microphotronics. These NLO properties can be further enhanced in low-dimensional semiconductors such as quantum wells,^[5] nanowires,^[4,6] or microstructures.^[7]

GaN is an ideal NLO material due to its high transparency in the visible wavelength.^[8] The optical nonlinearities in GaN are accessible at lower thresholds due to strong exciton binding energies and electron–phonon coupling.^[9] For harmonic generation, GaN nano- or microwires have been utilized,^[4] whereas 1D^[10] and 2D^[11,12] GaN photonic crystals based microcavities are utilized for electrodynamic-based nonlinear effects. The geometry of these NLO structures is usually isotropic along the length of propagation of the incident fundamental beam. Investigations of the linear optical properties of GaN pyramid structures have shown the presence of optical modes^[13] and lasing^[14] due to cavity formation and led to applications such as single-photon emitters^[15,16] and light-emitting diodes (LEDs).^[17] The growth of GaN can result in self-organized pyramid due to preferential growth of the atoms along $\{1\bar{1}01\}$ planes. The hexagonal cross sections of ZnO and GaN rods and tubes

1. Introduction

Non-centrosymmetric (NCS) structure in a crystal is essential for a finite second-order nonlinear coefficient^[1] for second-order NLO effects such as second harmonic generation (SHG). In a NCS crystal, the conversion efficiency of SHG is proportional to the square of the propagation length within the optical device, which necessitates longer length of NLO material and limits

S. Butler, Prof. A. Neogi
Institute of Fundamental and Frontier Sciences
University of Engineering Science
and Technology of China
Chengdu, China
E-mail: arup.neogi@unt.edu

S. Butler, Prof. A. Neogi
Institute of Fundamental and Frontier Sciences
Department of Physics
Advanced Manufacturing and Materials Processing Institute
University of Engineering Science and Technology
University of North Texas
Chengdu, Denton, TX 76203, USA

Prof. H. Jiang, Prof. J. Lin
Nanophotonics Center
Electrical and Computer Engineering
Whitacre College of Engineering
Texas Tech University
Lubbock, TX 79409-3102, USA

DOI: 10.1002/adom.201600804



have shown to confine microcavity modes for light trapped under appropriate conditions.^[18,19] This has led to the formation of whispering gallery modes (WGM) due to total internal reflection (TIR) in the horizontal plane^[20,21] or Fabry–Pérot modes in the axial plane or along the hexagonal facets in these microcavity structures.^[21,22] In crystalline high refractive index semiconductors quasi-WGMs can be supported that exhibit an ultrahigh- Q ^[23] and has been utilized in this work to enhance the second-order nonlinearity of the emitter.

As GaN is a high index material (≈ 2.56), the pyramid shape microcavities are ideal for enhanced TIR between the $\{1\bar{1}01\}$ facets. The hexagonal microcavity prefers modes with 60° angle of incidence within the cavity and reduces the mode degeneracy that can also result in non-WG modes such as the six bounce modes. The modes confined in a hexagonal microcavity are localized close to the rim of the resonator and therefore have small volumes. The high Q -factor and small interaction volume yield very high nonlinear conversion efficiency in hexagonal resonators.^[24,25] It results in a wider tunability of the fundamental mode at the SHG frequency in the hexagonal resonator that is not feasible in bulk crystals. Semiconductor cavities with varying diameters also showed different WGMs.^[20,26,27] Hexagonal GaN micropyramid structures in this study are highly transparent nonlinear media embedded into optical cavities. The shape and size of these wide bandgap nano- and microstructures are very critical. The apex of GaN pyramids scales down to a few nanometers and the multiphoton transition induced band-to-band excitons can be strongly confined at these tips. The tip acts as a nanoantenna located at the apex of the hexagonal cavity and is spatially anisotropic along the vertical dimension compared to optically isotropic structures such as hexagonal rods, disks, or thin films.

2. Results and Discussion

In this work, the light emission from a single individual GaN pyramid based microcavity in the presence of NLO interaction was investigated. The intensity of SHG and MPL emission generated with the microcavity was mapped for optical excitation along the symmetric axis of the GaN pyramid. By tuning the fundamental wavelength and power, both resonant and off-resonant nonlinear effects can be controlled. The NLO light generation was monitored in the axial direction to demonstrate the difference in the formation of cavity modes and the competing effects of the SHG and MPL processes in various planes

of the GaN pyramid microcavity. In the pyramid structures, the ultraviolet luminescence (UVL) due to multiphoton excitation (MPE) is more efficient from the apex of the pyramid, whereas the SHG in the backscattered direction is observed to be maximum at about 3–4 μm above the base of the pyramid. The nonlinearity observed within the bulk of the pyramid agrees well with the expected power dependence, whereas high-order power dependence observed at the tip of the pyramid influences the effective light generation from the microstructure. The second-order optical nonlinearity is observed to be significantly stronger in the pyramid structures due to the mode confinement within the cavity and results in a significantly higher efficiency of the overall light generation collected through the tip of the pyramid compared to axially homogeneous structures. The cavity modes in the hexagonal micropyramid were analyzed by analyzing the spatial interferometric fringes formed due to the confinement of the modes at the second harmonic of the fundamental frequency. The light emission from the single GaN micropyramid cavity can be controlled to realize a microphotonic source for hyperspectral imaging.

The array of GaN micropyramids was prepared by selective area epitaxial lateral overgrowth in a metal–organic chemical vapor deposition reactor. The GaN micropillars and epilayer used for comparison were grown at similar temperatures. Details of the fabrication process are reported in the Supporting Information. The surface morphology of GaN micropyramids was evaluated using scanning electron microscopy (SEM). Linear optical properties were studied using single-photon PL spectroscopy to compare the interband emission and the influence of defect states in the recombination of carriers from optical excited GaN micropyramids. NLO measurements (see the Supporting Information) were performed by tightly focusing a femtosecond near infrared (NIR) laser with 100 fs pulse width through a 0.9 numerical aperture (NA) objective to achieve high resolution with confocal sectioning. SHG and MPL were collected in the reflection geometry by an optical fiber coupled with a spectrometer equipped with a CCD detector.

A 2D array of selectively grown GaN hexagonal pyramids with semipolar $\{1\bar{1}01\}$ facets is shown in **Figure 1a**. The GaN pyramids were grown using SiO_2 masks. The mask was deposited on the GaN epilayer using plasma enhanced chemical vapor deposition (CVD) process and the dimensions of the windows on the mask were used to selectively control the growth of GaN micropyramids on the template.^[39,40] The circular openings in the SiO_2 mask, under optimum conditions, enabled the growth of hexagonal pyramids with six $\{1\bar{1}01\}$ converged planes

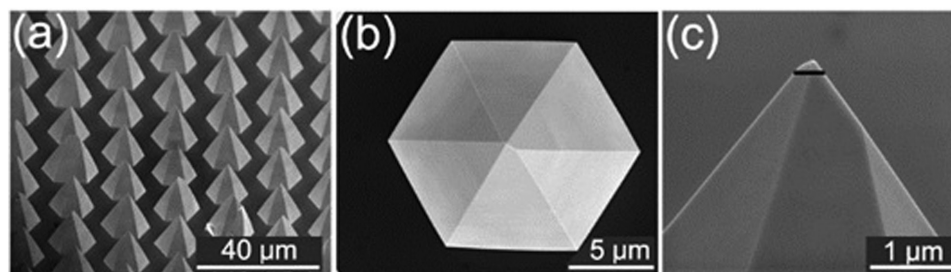


Figure 1. SEM images of GaN μ -pyramids grown on sapphire using selective lateral overgrowth. a) Tilted view of an array of GaN pyramids, b) top view of a single pyramid, and c) tilted view of the apex of a single pyramid. The black line at the tip of the pyramid is ≈ 200 nm.

as a direct consequence of the hexagonal characteristics of the wurtzite crystal. Semiconductors grown on substrates with lattice mismatch usually have defects induced within the crystal lattice at the interface during the growth process. Defects induced in crystal lattice can result in an increased second-order nonlinearity.^[41,42] Selective area epitaxial lateral overgrowth (SA-ELO) growth reduces defect density in the semiconductor compared to standard ELO growth process of epilayers.

The top view of a single pyramid (Figure 1b) shows six facets of the pyramid with extremely even surfaces as there is no etching involved, unlike top-down growth process. Individual pyramids have a base diameter and height of $\approx 15 \mu\text{m}$. The angle formed between the facet and SiO_2 mask is 62° . From Figure 1c, the sharp apex of the pyramid can be seen; the black line at the tip measures 210 nm. Occasionally, the convergence of the facets at apices of the pyramids are skewed forming a ridge due to the self-limited facet growth mechanism.^[28] The optical spot size used for NLO spectroscopy was significantly small compared to the dimension of the pyramid facets. The results presented in this work are probed along the symmetric axis of the pyramid. A slight deviation from the apex of the pyramid can introduce a significant change in the reflection and transmission properties of the incident light and subsequent collection of the nonlinear signal at the confocal plane of the detector. The sharp apex of the pyramid with subwavelength features can behave as nanoantennas and result in localization of electric fields and lead to modification of linear and NLO properties.^[29]

The ambient temperature PL spectrum of the GaN micro-pyramids excited above the bandgap using a single-photon excitation of wavelength 325 nm (3.81 eV) is shown in Figure 2a. The carrier densities were estimated to be $2 \times 10^{21} \text{ cm}^{-3}$ for 325 nm excitation. The PL spectrum shows an asymmetric UVL peak centered at 374 nm (3.32 eV) with a shoulder at 365 nm (3.4 eV). The peak at 365 nm is attributed to band-to-band transition,^[9] whereas the peak at 374 nm could be caused by electro-hole plasma emission^[30,31] due to high carrier concentration. A broad visible band centered at 560 nm (2.21 eV), commonly referred to as the yellow luminescence (YL) band is also observed. This is attributed to recombination involving shallow donors and deep acceptors; likely due to Ga vacancies.^[9]

Figure 2b represents the spectra of GaN pyramids pumped by the NIR laser at 720, 770, 840, and 900 nm (1.72, 1.61, 1.48, and 1.38 eV) wavelengths from the same spot on the sample at constant power. Because the energies of the excitation photons are well below the bandgap energy of GaN ($E_g = 3.4 \text{ eV}$), the observed luminescence bands are due to MPE. This MPE process involves the simultaneous interaction of two or three identical photons via states within the bandgap of the material, producing an absorption event equivalent to that of a single photon having twice or thrice the energy. Spectral measurements of GaN pyramid produce emission peak positions with similar energy for both single and multiphoton excitations. Therefore, the origin of the recombination mechanism involved in the NLO emission process is identical to the linear process. Comparing the UVL peak wavelength to the NIR laser excitation wavelengths, we observed that the excitation energy (E) at 720 nm is almost half the E_g of GaN, whereas excitation energies at 770, 840, and 900 nm are less than half but more than one-third of the E_g .

Figure 2c shows the energy of the excitation relative to the bandgap of GaN. It is likely that the UVL originates from a two-photon absorption (2PA) process for 720 nm excitation and from a three-photon absorption (3PA) process for 770, 840, and 900 nm excitations. In the case of a two-photon absorption process, an electron in the valence band absorbs two photons through virtual energy levels and transfers to the conduction band. The electron relaxes to the bottom of the conduction band via longitudinal optical phonon scattering and recombines spontaneously with the holes in the valence band through a radiative process, resulting in UVL. The efficiency of a 2PA process is higher than a 3PA process, which consequently results in a higher emission intensity of the UVL due to 720 nm compared to 770, 840, or 900 nm wavelength excitations as observed in Figure 2b. Moreover, the third-order interband nonlinearity is also maximum when the excitation wavelength is resonant to the semiconductor bandgap. Any SHG signal generated at 720 nm is absorbed efficiently by the absorbing medium. For excitations with wavelengths 770, 840, and 900 nm, a narrow peak is also observed at half the excitation wavelength (twice the incident frequency) indicating SHG of the incident light within the pyramid. The full-width at half-maximum (FWHM)

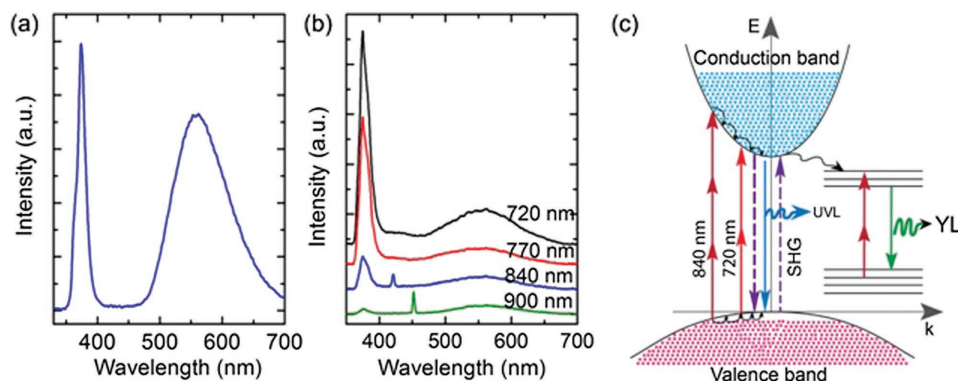


Figure 2. Light emission from micropyramids. a) Single photon excited photoluminescence spectrum from an array of micropyramids by a continuous wave laser at 325 nm, b) multiphoton induced photoluminescence spectra from a single micropyramid excited by a femtosecond laser at 720 nm (black), 770 nm (red), 840 nm (blue), and 900 nm (green) at constant power, and c) schematic of a simplified band diagram depicting the nonlinear carrier transition processes observed in the bandgap of GaN resulting in UV and YL bands. All the spectra were taken at ambient temperature.

of SHG spectral peaks for excitations at 770, 840, and 900 nm is measured to be about 4 nm, which is approximately equal to $1/\sqrt{2}$ of FWHM of the transform limited band width of the fundamental beam.

The origin of NLO light generation at various excitation wavelengths is investigated by power-dependent measurements. The intensity of the nonlinear process on the incident pump density follows a power law; $I_{\text{MPL}} = I_{\text{p}}^n$, where n is the number of photons required to induce the effect, I_{MPL} and I_{p} are intensities of emission and excitation, respectively. Therefore, to determine the photon contribution involved, intensity dependence of the UVL, SH, and YL as a function of incident power of the pump laser was measured and is shown in Figure 3. The contributions are estimated from the log-log scale in Figure S4 (Supporting Information). Both the luminescence bands exhibit different exponents for above and below $E_{\text{g}}/2$ excitation. For 720 nm excitation ($E > E_{\text{g}}/2$), power law exponent $n \approx 2$ indicates that the UVL band is induced by a two-photon process; whereas, for 770–900 nm, UVL band is induced by a three-photon process as $n \approx 3$ (Figure 3d). Theoretical values of the exponent are 2 and 3 for 2PA and 3PA. This is reasonable considering the high power density achieved by tight focusing of the incident beam, increasing the possibility of interband transitions to be excited via two or three-photon absorption. On the other hand, the power law exponent shows that YL band is a consequence of a single-photon process for 720 nm excitation and a gradual increase to two-photon process for 900 nm excitation. Toda et al.^[32] observed a power law exponent of $n = 1.5$ for YL at 720 nm excitation from freestanding bulk GaN with a thickness of 420 μm . They attributed it to a combination of two processes: (1) a two-photon excitation into the conduction band, where the excited carriers relax to the YL band emitting luminescence, and (2) a linear transition within the yellow band contributing to YL. In the present experiments, the exponent value of $n = 1$ suggests the presence of the latter case. We believe that major contribution to YL is from the linear absorption of SHG photons with a wavelength close to the absorption edge of the GaN pyramids created by the 720 nm excitation (purple arrow in Figure 2c). In addition, PLE measurements (see Figure S2, Supporting Information) for YL detection energy show the

absorption edge to be around 360 nm. For excitation at 900 nm, YL band is purely due to a two-photon process. Efficient 2PA in the YL band was observed in previous studies^[32] because of the presence of deep level states at around 1.3 eV above the valence band. Presence of such midgap states can enhance the probability of 2PA in the YL band. Therefore, when the excitation wavelength is sufficiently detuned from resonance, the shallow levels can be directly populated by electrons in the valence band by means of coherent 2PA. For excitations at 770 and 840 nm, a combination of dominant 2PA in the YL band and the re-absorption of photons emitted due to the interband transition by the defect level states is likely to yield the observed exponents of 1.7 and 1.8, respectively.

During intensity-dependent measurements, we observed that the power law exponent for the luminescence peaks showed a difference toward the apex position of the pyramid (see Figure 3b and Figure S4, Supporting Information). Measurements at the apex were made within 2 μm distance from the apex of the pyramid. The dimension of the apex of the pyramid as seen from Figure 1c is much smaller compared to the excitation wavelengths. The value of n for UVL at the apex was an exponent higher than the value observed in the bulk of the pyramid. The increase in power exponent could be a result of transition from the electron–hole plasma (EHP) to stimulated emission, which is reasonable because the carrier densities created by the MPE energies are of the order of 10^{22} cm^{-3} . Moreover, localization of electric fields created by the subwavelength tapered geometry of the dielectric pyramid at the apex can result in multipole effects thereby enhancing the directionality of the emission.^[33,34] As the exponent value increased for UVL, a reduction in the power exponent to YL peak was also observed due to a saturation of absorption in the YL band. Decrease in power exponent for YL at the apex for off resonant excitation energies confirms the presence of a complex emission process in the YL band. A significant deviation in the exponent for SHG at 770 nm could be due to coupling of UVL and SHG or uncertainties in deconvoluting the SHG peak from UVL.

Spatially resolved MPL and SHG measurements were performed to evaluate the effects of dimensionality and crystal quality on the NLO emission process. Spatial measurements were made in the direction of the optic axis. In addition, confocal multiphoton imaging was performed to study the effect of the hexagonal cavity on the nonlinear light generation process. Both SHG and MPL processes critically depends on the interaction/absorption cross section of the medium. As the excitation volume changes from a few hundred nanometers at the apex to $\approx 15 \mu\text{m}$ at the base of the pyramid, the light–matter interaction is significantly modified by the shape and size of the GaN pyramid. The NLO signal generated from a single pyramid is therefore collected over the entire height of the pyramid to characterize the effect of the changes in structural composition and symmetry of the structure on the NLO processes within the semiconductor.

Figure 4 represents the spatial measurements carried out at 720, 840, and 900 nm excitation wavelengths with same input power density. The results show significant UVL and YL throughout the pyramidal volume for 720 nm excitation (Figure 4b) with UVL being maximum at the apex of the pyramid. The YL has a uniform intensity profile throughout the

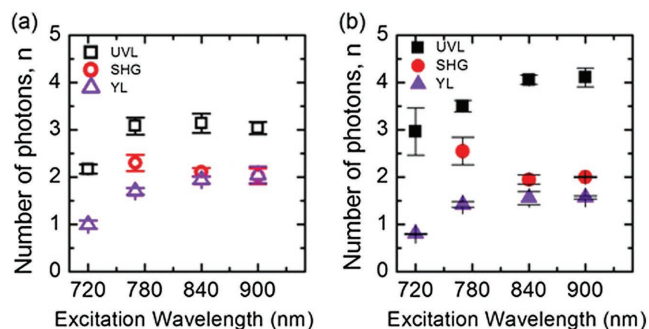


Figure 3. Excitation intensity dependence on SHG and MPL as a function of excitation wavelength. a) Number of photons involved in the transition as a function of excitation wavelength for UVL (black square), YL (purple diamond), and SHG (red circle) at the center of the symmetric axis averaged over six single pyramids, and b) number of photons involved in the transition as a function of excitation wavelength at the apex of the pyramid averaged over six single pyramids.

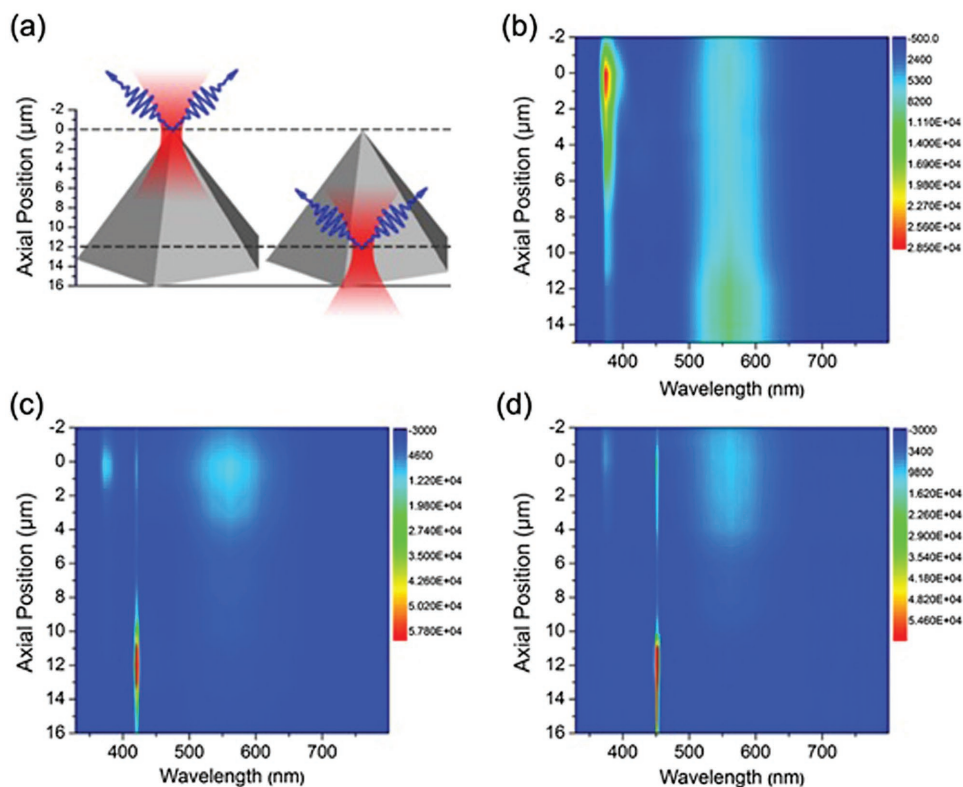


Figure 4. 2D plots of line scan of multiphoton induced luminescence and second harmonic generation as a function of pyramid's symmetric axis. a) Two representative laser excitation positions along symmetric axis of the pyramid. Spatially dependent light generation from pyramid using b) 720, c) 840, and d) 900 nm excitation.

pyramidal volume, except for a small increase at the base. The increase in the structural defects at the base^[35,36] is the likely cause of the increased YL emission. At 720 nm excitation, SHG generated at 360 nm results in the linear absorption of SHG photons into conduction band and subsequent relaxation to shallow states followed by recombination in the shallow donor-deep acceptor states resulting in the increase in YL toward the base. In addition, the structural defects at the base can also contribute to increased crystalline non-centrosymmetry, increasing the probability of SHG. For excitations at 840 and 900 nm, both second-order and third-order nonlinear effects were observed at the apex of the pyramid (see Figure 4c,d). Unlike 720 nm excitation, the intensity of both emission bands is higher at the apex and decreases toward the base of the pyramid. SHG signal is also present at the apex; however, maximum SHG intensity is observed at about 4 μm above the base. For excitation powers below a threshold power of 10 mW, only SHG is generated in the bottom half of the pyramid structure for 840 and 900 nm excitation.

From Figure 4, it is clear that the second-order nonlinearity is higher at a position 4–5 μm above the base, whereas third-order nonlinearity is higher toward the apex. Detailed structural analysis of similar GaN pyramids mostly saw threading dislocations at the base and nearly defect-free areas were observed in the lateral grown regions away from the mask openings.^[35] A combination of the geometrical effects increasing nonlinearly induced dipole moments, increased crystal quality, and high carrier concentration are likely to enhance the emission signals

at the apex. Increase in SHG intensity toward the base can be attributed to mainly two reasons: (1) the length of the microp pyramid is within a few coherence lengths ($\approx 3 \mu\text{m}$ for GaN for 840 nm), and (2) the $\{1\bar{1}01\}$ facets of the high refractive GaN pyramid ($n = 2.5\text{--}2.67$) facilitates total internal reflection of the incident infrared light and is ideal to form cavity resonators with high optical nonlinearity. The optical nonlinearity is usually maximum at the resonance when the fundamental or the generated frequencies are tuned to the bandedge or the excitonic level of the semiconductor. For second harmonic waves below the bandgap or the excitonic states, the nonresonant optical nonlinearity is not only relatively small but also accompanied by very small attenuation. For the less attenuated modes of the hexagonal resonators, which belong to a class of open resonators provide the photons confined in the cavity a better probability to interact without being absorbed or dispersed. The six-dot pattern was observed only for off-resonant frequencies (Figure 5c), specifically for fundamental excitation wavelengths longer than 810 nm. The intensity of the second harmonic frequency confined within the cavity decreases away from the optimal position in the axial direction. Any dissipation due to excitonic or the bandgap states destroys the cavity mode confinement. Even without strong non-centrosymmetry of the crystal, the hexagonal resonator can enhance the SHG process due to increased interaction length of the electromagnetic mode with the nondissipative medium. It is also observed from Figure 2c that the SHG efficiency is more at 900 nm compared to 840 nm.

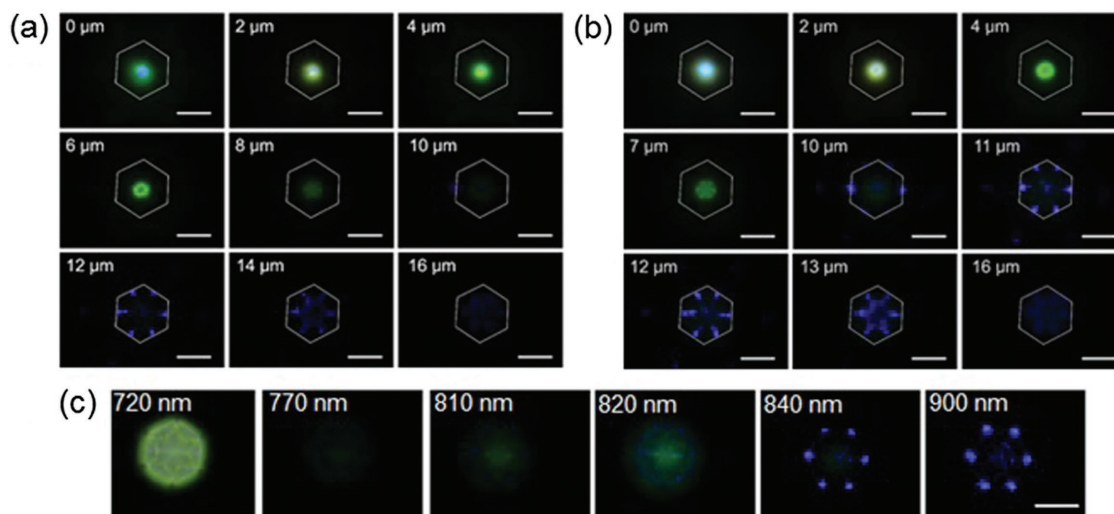


Figure 5. Vertical emission light profile demonstrating spatial control of light emission from a GaN micropillar with excitation at 840 nm from the same pillar: a) 15 mW power at the sample and b) 30 mW power at the sample. Image labeled 12 μm in (a) corresponds to the red curve in Figure S1 (Supporting Information). White hexagon outlines the pillar base. In these images, 0 μm is the spatial position at apex, and 16 μm is the base. c) Excitation wavelength dependent emission profile within a GaN micropillar at $\approx 11 \mu\text{m}$ position. Scale bar represents 10 μm .

By comparing Figures 5a and 4c, we observed that MPE-induced spontaneous UVL and YL dominate the emission from the apex of the GaN pyramid. For excitation depths at around 2–3 μm into the pyramid, the effective emission is dominated by YL. At higher pump intensity (Figure 5b), the UVL intensity increases relatively more than the YL intensity and results in a relatively cool-white emission at the apex. However as the spontaneous emission due to UVL decreases within the pyramid plane with larger radius, one can observe formation of stable modes at the mid-point of the $\{1\bar{1}01\}$ facets of GaN. Because the refractive index of GaN is larger than air, the generated SHG at 420 nm is confined within the pyramid by TIR, where the relative refractive index is defined as $\tilde{n} = n/n_0 > 1$. The mode of frequencies trapped in the pyramid is similar to the quasi-WGM modes. It can be observed from all the images of the GaN pyramid (Figure 5a,b). For depths exceeding 10 μm , the generated second harmonic signal have six reflections with identical path length ($S_6 = 3\sqrt{3}Rn$) and with a 60° angle of incidence to the facet normal. The spontaneous emission from the defects (YL) appears to illuminate the basal plane at higher pump densities. The SHG modes appear to be confined tightly in a small mode volume close to the facet of the pyramid at an 11–14 μm depth where the SHG intensity is observed to be maximum. This quasi-WGM mode exhibits a high- Q that contributes to enhanced SHG within the pyramid. Such an effect can be attributed to the pyramidal shape of the GaN microstructure as no mode confinement due to cavity modes are observed in the reference GaN micropillars under our experimental condition.

A closer observation of the confined modes at high pump intensities shows the additional modes with varying radius. The inner mode is the SHG mode and the outmode is presumably the mode from the multiphoton process. In a hexagonal resonator, the contribution due to geometrical dispersion results in a negative Δn , where $\Delta n = \tilde{n} - n$. The optical field concentrated inside the hexagonal resonator is usually located at some

distance away from the facet due to dispersion. The optical path length is shorter than $3\sqrt{3}Rn$ due to this geometrical dispersion ($d\Delta n(\lambda)/d\lambda < 0$). Therefore, at longer wavelengths more of the optical power is carried by the evanescent field outside the resonator and thereby reducing the effective refractive index. Consequently, the effective radius of the SHG mode is smaller than the UVL mode, which forms closer to the facet. However, as we move closer to the substrate the SHG intensity is reduced due to weaker confinement of the cavity mode as the electromagnetic waves are evanescently leaked out into the GaN/SiO₂ interface layers at the base. Also at the apex of the pyramid, the sharp edges of the hexagonal faces result in leaky modes and reduce the confinement of the SHG signal confined within the cavity. A qualitative analysis of the mode confinement within a hexagonal pyramid is shown in Section S3 (Supporting Information).

The average powers of incident and SHG fields were measured and the experimental second harmonic conversion efficiency of the pyramid was estimated. Figure 6a shows the SHG power as a function of the incident pump power at 12 μm position on the symmetric axis of the pyramid, where maximum intensity of the SHG signal was observed. The measurements were made at an incident fundamental wavelength of 840 nm. The MPL contribution was filtered using a 420 nm interference filter with a bandwidth of 10 nm. Figure 6b depicts the efficiency of the SHG process, η , as a function of the incident pump power. The SHG efficiency is estimated as $\eta = P_{2\omega}/P_\omega$ where $P_{2\omega}$ and P_ω are the measured average powers of the SHG and incident pump beams. The scattering of fundamental and SHG beams was not included in this estimation. Figure 5b shows that the SHG efficiency scales linearly with the incident pump power. A conversion efficiency of 1.1×10^{-7} was obtained at about 4 μm above the base of the pyramid for a pump power of 24 mW compared to 1.4×10^{-5} (at 21 mW) obtained from ZnO nanorods,^[37] 1.8×10^{-9} (at 3 mW) from Au-coated silica nanoparticles,^[38] and 2.4×10^{-9} (7 mW) for a GaN 2D photonic

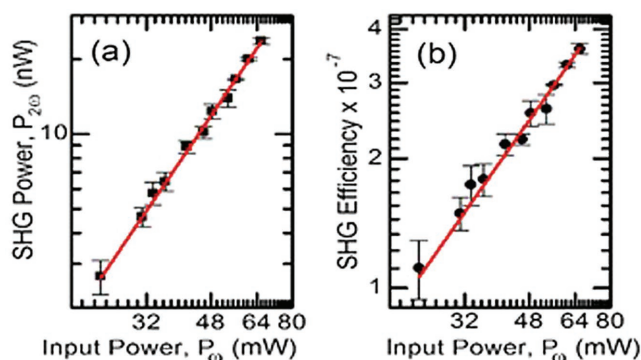


Figure 6. Experimental power measurements at SHG wavelength of 420 nm. a) Average SHG power, $P_{2\omega}$ versus incident pump power, P_{ω} . b) SHG efficiency, η , as a function of incident pump power at 840 nm.

crystal.^[11] It should be noted that these comparisons are made for our structures using pulsed excitation of the fundamental laser source.

3. Conclusions

In conclusion, GaN micropyramidal structures with $\{1\bar{1}01\}$ facets were formed on patterned substrates by metal–organic chemical vapor deposition (MOCVD) using ELO growth technique. Color temperature and coherence of the light generation from the pyramid can be controlled by selective onset of the nonlinear process which depends not only on the incident laser energy and intensity but also on the geometry of the micropyramid. Quasi-WGM like modes were observed for off-resonant excitations from the GaN micropyramid. Multiphoton transition induced by tightly focused femtosecond NIR radiation results in UVL due to EHP and defect level mediated YL from GaN micropyramids. The MPL due to 2PA is stronger at the interband resonance when the energy of incident field corresponds to half the bandgap energy of GaN. The efficiency of the MPL is observed to be maximum at the apex of the pyramid. For excitation below the bandgap energy, in the absence of any two-photon absorption, second harmonic signals are generated from these pyramids. The SHG from micropyramid confirmed by a quadratic power dependence was observed to have maximum intensity at about 3–4 μm above the base of the pyramid. The results indicate that GaN micropyramids have large third-order optical nonlinearity due to dimensional effects and crystalline quality at the apex. However, second-order nonlinearity is larger where the cavity modes are confined. The axial inhomogeneity in the micropyramid provides hexagonal cross-section slices with varying diameters offering flexible WGM conditions for a range of wavelengths. Cavity formation along with NLO light generation and controlled growth of GaN based micropyramids show potential for all optic circuitry applications.

4. Experimental Section

Material Growth and Fabrication: The array of GaN micropyramids was prepared by SA-ELO in a MOCVD reactor. A micrometer thick GaN epilayer was grown on a *c*-plane sapphire substrate with a 100 nm AlN

buffer layer. Site-controlled GaN microstructures were grown using a 200 nm SiO₂ masking layer.^[39,40] An array of circular holes with 5 μm diameter and 20 μm pitch was fabricated by photolithography and dry etching techniques. GaN micropyramids were then selectively grown on the patterned substrate in a MOCVD chamber at 1050 °C with ammonia (NH₃) and triethylgallium (TEG) as reactants with hydrogen as carrier gas. During the 3 h lateral overgrowth process, NH₃ flow rate was maintained at 1.8 slm, whereas TEG flow rate was varied from 1.8 $\mu\text{mol min}^{-1}$ for the first hour to 5.3 $\mu\text{mol min}^{-1}$ for the remaining 2 h of growth process. The circular openings in the SiO₂ mask, under optimum conditions, enabled the growth of hexagonal pyramids with six $\{1\bar{1}01\}$ converged planes as a direct consequence of the hexagonal characteristics of the wurtzite crystal.

Optical Characterization Methods: The surface morphology of GaN micropyramids was evaluated using SEM using a FEI Nova Nanolab 200 with a 5 kV electron beam. Linear optical properties were studied using single-photon PL spectroscopy, where single-photon optical excitation was achieved using the 325 nm line from a continuous wave helium-cadmium laser of 15 mW focused to a 100 μm diameter spot size on the sample. The incident beam was at a 45° angle from the normal of the sample substrate. The PLE measurements were performed using a white-light scanning source along with the detector fixed to the maximum PL wavelength. The gain of the detector was normalized for the scan range of the wavelength under study.

The nonlinear optical measurements were performed by tightly focusing a femtosecond pulsed NIR light through a high NA objective to achieve high resolution with confocal sectioning. The NIR excitation source was a tunable Ti:sapphire laser with pulse width of 100 fs and repetition rate of 80 MHz. The excitation wavelengths for multiphoton experiments were chosen to be 720, 770, 840, and 900 nm. The incident NIR excitation beam was tightly focused on the sample using a 0.9 NA objective. The resulting experimental beam waist was measured by taking the FWHM of a 1D intensity histogram across centroid of a lower fluence laser spot on the imaging plane of the CCD. The measurements show that the excitation beam waist was ≈ 600 nm for 840 nm. The sample was mounted on a microscope stage that allowed XYZ positioning of the sample with ≈ 500 nm resolution. A variable attenuator was used to control the power of the incident laser on the sample. MPL was collected in the reflection geometry by an optical fiber coupled with a spectrometer equipped with a back thinned CCD detector. A 350–670 nm interference band pass filter was used to block the laser beam from entering into the spectrometer.

Supporting Information

Supporting Information is available from the Wiley Online Library or from the author.

Acknowledgements

The authors thank Prof. Arkadii Krokhin and Mr. Andrey Bozko for assistance with numerical simulation.

Received: October 1, 2016
Revised: November 18, 2016
Published online:

- [1] Y. R. Shen, *The Principles of Nonlinear Optics*, Wiley, New York 1984.
- [2] M.-L. Ren, R. Agarwal, W. Liu, R. Agarwal, *Nano Lett.* **2015**, *15*, 7341.
- [3] G. Bautista, J. Mäkitalo, Y. Chen, V. Dhaka, M. Grasso, L. Karvonen, H. Jiang, M. J. Huttunen, T. Huhtio, H. Lipsanen, M. Kauranen, *Nano Lett.* **2015**, *15*, 1564.
- [4] J. P. Long, B. S. Simpkins, D. J. Rowenhorst, P. E. Pehrsson, *Nano Lett.* **2007**, *7*, 831.

- [5] A. Hayat, P. Ginzburg, M. Orenstein, *Nat. Photonics* **2008**, 2, 238.
- [6] Y. Nakayama, P. J. Pauzauskie, A. Radenovic, R. M. Onorato, R. J. Saykally, J. Liphardt, P. Yang, *Nature* **2007**, 447, 1098.
- [7] S. Mariani, A. Andronico, A. Lemaître, I. Favero, S. Ducci, G. Leo, *Opt. Lett.* **2014**, 39, 3062.
- [8] O. Ambacher, *J. Phys. D: Appl. Phys.* **1998**, 31, 2653.
- [9] M. A. Reshchikov, H. Morkoç, *J. Appl. Phys.* **2005**, 97, 61301.
- [10] J. Torres, D. Coquillat, R. Legros, J. P. Lascaray, F. Teppe, D. Scalbert, D. Peyrade, Y. Chen, O. Briot, M. L. V. d'Yerville, E. Centeno, D. Cassagne, J. P. Albert, *Phys. Rev. B* **2004**, 69, 85105.
- [11] Y. Zeng, I. Roland, X. Checoury, Z. Han, M. E. Kurdi, S. Sauvage, B. Gayral, C. Brimont, T. Guillet, M. Mexis, F. Semond, P. Boucaud, *Appl. Phys. Lett.* **2015**, 106, 81105.
- [12] D. Coquillat, G. Vecchi, C. Comaschi, A. M. Malvezzi, J. Torres, M. L. V. d'Yerville, *Appl. Phys. Lett.* **2005**, 87, 101106.
- [13] H. X. Jiang, J. Y. Lin, K. C. Zeng, W. Yang, *Appl. Phys. Lett.* **1999**, 75, 763.
- [14] S. Bidnyk, B. D. Little, Y. H. Cho, J. Krasinski, J. J. Song, W. Yang, S. A. McPherson, *Appl. Phys. Lett.* **1998**, 73, 2242.
- [15] P. R. Edwards, R. W. Martin, I. M. Watson, C. Liu, R. A. Taylor, J. H. Rice, J. H. Na, J. W. Robinson, J. D. Smith, *Appl. Phys. Lett.* **2004**, 85, 4281.
- [16] A. Lundskog, C.-W. Hsu, K. Fredrik Karlsson, S. Amloy, D. Nilsson, U. Forsberg, P. O. Holtz, E. Janzén, *Light: Sci. Appl.* **2014**, 3, e139.
- [17] W. Chen, G. Hu, J. Jiang, M. Liu, Y. Yang, P. Xiang, G. Hu, Y. Lin, Z. Wu, Y. Liu, B. Zhang, *J. Disp. Technol.* **2015**, 11, 285.
- [18] C. Czékalla, T. Nobis, A. Rahm, B. Cao, J. Zúñiga-Pérez, C. Sturm, R. Schmidt-Grund, M. Lorenz, M. Grundmann, *Phys. Status Solidi B* **2010**, 247, 1282.
- [19] J. Lu, C. Xu, J. Dai, J. Li, Y. Wang, Y. Lin, P. Li, *ACS Photonics* **2015**, 2, 73.
- [20] H. Dong, Z. Chen, L. Sun, J. Lu, W. Xie, H. H. Tan, C. Jagadish, X. Shen, *Appl. Phys. Lett.* **2009**, 94, 173115.
- [21] P.-M. Coulon, M. Hugues, B. Alloing, E. Beraudo, M. Leroux, *Opt. Express* **2012**, 20, 18707.
- [22] H. Kudo, *Phys. Rev. A* **2013**, 88, 023807.
- [23] I. S. Grudin, Ph.D. Thesis, *California Institute of Technology*, Pasadena, CA, USA **2008**.
- [24] V. S. Ilchenko, A. A. Savchenkov, A. B. Matsko, L. Maleki, *Phys. Rev. Lett.* **2004**, 92, 43903.
- [25] D. V. Strekalov, C. Marquardt, A. B. Matsko, H. G. L. Schwefel, G. Leuchs, *J. Opt.* **2016**, 18, 123002.
- [26] T. Nobis, E. M. Kaidashev, A. Rahm, M. Lorenz, M. Grundmann, *Phys. Rev. Lett.* **2004**, 93, 103903.
- [27] Y. Zhang, H. Zhou, S. W. Liu, Z. R. Tian, M. Xiao, *Nano Lett.* **2009**, 9, 2109.
- [28] A. Lundskog, U. Forsberg, P. O. Holtz, E. Janzén, *Cryst. Growth Des.* **2012**, 12, 5491.
- [29] P. Reichenbach, L. M. Eng, U. Georgi, B. Voit, *J. Laser Appl.* **2012**, 24, 42005.
- [30] S. Krotkus, S. Miasojedovas, S. Juršėnas, *Phys. B: Condens. Matter* **2014**, 450, 16.
- [31] C. Cachoncinlle, E. Millon, A. Petit, *Opt. Commun.* **2016**, 368, 49.
- [32] Y. Toda, T. Matsubara, R. Morita, M. Yamashita, K. Hoshino, T. Someya, Y. Arakawa, *Appl. Phys. Lett.* **2003**, 82, 4714.
- [33] A. E. Krasnok, C. R. Simovski, P. A. Belov, Y. S. Kivshar, *Nanoscale* **2014**, 6, 7354.
- [34] R. Guo, E. Rusak, I. Staude, J. Dominguez, M. Decker, C. Rockstuhl, I. Brener, D. N. Neshev, Y. S. Kivshar, *ACS Photonics* **2016**, 3, 349.
- [35] T. S. Zheleva, O.-H. Nam, M. D. Bremser, R. F. Davis, *Appl. Phys. Lett.* **1997**, 71, 2472.
- [36] J. K. Farrer, C. B. Carter, *J. Mater. Sci.* **2006**, 41, 779.
- [37] W. Liu, K. Wang, H. Long, S. Chu, B. Wang, P. Lu, *Appl. Phys. Lett.* **2014**, 105, 71906.
- [38] Y. Zhang, N. K. Grady, C. Ayala-Orozco, N. J. Halas, *Nano Lett.* **2011**, 11, 5519.
- [39] S. Kitamura, K. Hiramatsu, N. Sawaki, *Jpn. J. Appl. Phys.* **1995**, 34, L1184.
- [40] W. Yang, S. A. McPherson, Z. Mao, S. McKernan, C. B. Carter, *J. Cryst. Growth* **1999**, 204, 270.